Journal of Power Sources 196 (2011) 10430–10441

Contents lists available at ScienceDirect

Journal of Power Sources

journal homepage: www.elsevier.com/locate/jpowsour

Solar photovoltaic charging of high voltage nickel metal hydride batteries using DC power conversion

Nelson A. Kelly*, Thomas L. Gibson

General Motors R&D Center, 480-106-224, Chemical Sciences and Materials Systems Laboratory, 30500 Mound Road, Warren, MI 48090-9055, USA

ARTICLE INFO

Article history:
Received 10 June 2011
Received in revised form 11 July 2011
Accepted 12 July 2011
Available online 23 July 2011

Keywords:
Photovoltaic
High voltage battery
Solar energy
Electric vehicles
Optimized system

ABSTRACT

There are an increasing number of vehicle choices available that utilize batteries and electric motors to reduce tailpipe emissions and increase fuel economy. The eventual production of electricity and hydrogen in a renewable fashion, such as using solar energy, can achieve the long-term vision of having no tailpipe environmental impact, as well as eliminating the dependence of the transportation sector on dwindling supplies of petroleum for its energy. In this report we will demonstrate the solar-powered charging of the high-voltage nickel-metal hydride (NiMH) battery used in the GM 2-mode hybrid system. In previous studies we have used low-voltage solar modules to produce hydrogen via the electrolysis of water and to directly charge lithium-ion battery modules. Our strategy in the present work was to boost low-voltage PV voltage to over 300 V using DC–DC converters in order to charge the high-voltage NiMH battery, and to regulate the battery charging using software to program the electronic control unit supplied with the battery pack. A protocol for high-voltage battery charging was developed, and the solar to battery charging efficiency was measured under a variety of conditions. We believe this is the first time such high-voltage batteries have been charged using solar energy in order to prove the concept of efficient, solar-powered charging for battery-electric vehicles.

1. Introduction

A major transformation for the automobile, referred to as a "new DNA", can be achieved by moving from the present mechanical system powered by petroleum to a system energized by electricity and powered by electric motors [1–3]. This can be achieved by utilizing fuel cells and hydrogen, i.e., fuel cell electric vehicles (FCEV) and/or by utilizing batteries, i.e., battery electric vehicles (BEV). An interim stage between the present vehicles and the future electrically-powered vehicles is represented by hybrid electric vehicles (HEV) and extended range electric vehicles (EREV) in which internal combustion engines and electric motors are both utilized. Both HEV and EREV offer improved fuel economy versus vehicles powered by standard internal combustion engines [4–8].

Reducing petroleum usage in order to make the dwindling petroleum supply last longer, and reducing the emissions of air pollutants and carbon dioxide, are key ingredients to improving vehicle powertrains by electrification [1–3,9]. If the electricity can be supplied by using a renewable form of energy, such as wind or solar, then the transportation system can become sustainable and virtually pollution free with respect to tailpipe emissions [1–3,9–21].

Currently GM has an aggressive program to improve fuel economy, reduce tailpipe emissions, and displace petroleum usage by introducing hybrid, battery, and fuel cell powered electric drive systems. At present, GM has 2-mode hybrid vehicles in the market that use battery electric motors to assist the IC engine as well as capture and store energy during braking in order to increase the vehicle fuel efficiency. GM is now selling an EREV with rechargeable plug-in battery packs called the Chevrolet Volt. And, GM has the largest test fleet (over 100) of FCEV currently on the road and with the Chevrolet Equinox FCEV. However, in order to remove vehicles from contributing to environmental pollution it is necessary to begin a transition to using renewable energy to charge the batteries in electric vehicles or to produce the hydrogen for fuel cell electric vehicles. One way in which vehicles with electric powertrains can achieve such a goal is by using hydrogen powered fuel cells and battery-powered electric vehicles in which the hydrogen and/or battery charge is provided by solar power such as photovoltaic (PV) arrays.

Solar battery charging can provide pollution-free energy for extended range electric and pure electric vehicles [11]. Since battery packs for such vehicles will have electronic controls to monitor and control the charging, the PV system only needs to be designed to have a maximum-power point voltage slightly above the charge cut-off voltage programmed into the battery pack control module.

We have studied the use of photovoltaic (PV) solar energy for producing hydrogen as well as charging batteries [9]. For example,

* Corresponding author. Tel.: +1 586 986 1623; fax: +1 586 986 1910.
E-mail address: nelson.a.kelly@gm.com (N.A. Kelly).

0378-7753/$ – see front matter © 2011 Elsevier B.V. All rights reserved.
doi:10.1016/j.jpowsour.2011.07.043

we built and tested a system for producing high-pressure hydrogen for fueling FCEV that uses solar energy and the electrolysis of water [11]. That system was a proof of concept for a home hydrogen fueling system. The solar hydrogen fueling system utilized an optimized direct connection between the photovoltaic (PV) solar and electrolyzer systems [10]. By designing the two systems to have a maximized coupling, a solar to hydrogen energy efficiency of nearly 10%, versus previous systems with less than 6% efficiency, was attained. In a similar manner we have demonstrated the optimized direct solar PV charging of lithium-ion batteries; for those tests the solar to electric battery charging efficiency reached 14% [11]. The use of such systems in distributed energy systems for FCEV and BEV/EREV was described in an earlier publication [9].

Although we have charged lithium-ion batteries using PV electricity, our earlier work on battery charging used relatively low DC voltages (<60 V). However, to charge the batteries in BEV and The batteries in EREV will require DC voltages of over 300 V for charging, and in fact, most popular HEV use batteries with such high voltages. As a first step in charging high-voltage batteries we decided to use our low voltage arrays with a DC–DC converter to increase the voltage to that necessary to charge HEV high-voltage batteries. Based on inputs from GM battery and electric powertrain experts, we decided to use the nickel metal hydride (NiMH) battery in the GM 2-mode hybrid as the first high-voltage battery to be charged with PV electricity as a proof of concept. High-voltage NiMH batteries were used in the later versions of GMs EV-1, and are presently used in the GM-Allison hybrid bus and the GM 2-mode hybrid trucks, as well as the most widely sold hybrid vehicle, the Toyota Prius. To our knowledge, this is the first time a high-voltage HEV battery has been charged using solar energy.

The impetus for DC charging of the vehicle is threefold; (1) it eliminates the approximately 10% loss for conversion of AC to DC, (2) it eliminates the cost of AC–DC of power converters, and (3) it could eliminate the weight of the on-board charger in a vehicle such as the Chevrolet Volt, which in turn will improve the vehicle fuel efficiency and result in a greater vehicle driving range. However, direct DC battery charging will require an interface on the vehicle for connecting the DC power to the battery pack, as well as a means for utilizing the battery pack control module to wake up the pack and regulate the battery charging.

High-voltage vehicle batteries may also be used at their end of life for energy storage on the grid [20]. The U.S. grid presently has little stored electrical energy, and must maintain spinning reserves to maintain its ability to respond to sudden loads. Renewable electricity put onto the grid may worsen the problem of regulation on the grid, and storage of electrical energy as hydrogen or in batteries is one option to deal with the problem. So, in addition to solar PV charging of vehicle high voltage batteries in the vehicle, there is the possibility of charging them in an energy storage bank.

Solar energy can provide a clean, renewable source of energy to charge plug-in electric vehicles such as the Volt EREV and maximize the environmental benefits of eliminating green house gases and other emissions. A major challenge to using solar energy technology is the need to design an inexpensive, safe solar battery charger with optimum efficiency. Most solar systems utilize low voltage, and one way to boost the voltage to that needed to charge the 300 V NiMH batteries used in hybrid and electric vehicles is to utilize DC–DC conversion. This work measures the characteristics of such a system.

2. Experimental

The system was designed as a number of units that take solar energy and use it to charge a hybrid electric vehicle (HEV) battery. Some of the parts were used previously, while other parts had to be designed and built in order to charge a high-voltage battery. The following will describe the system components and their interworkings.

Table 1
Solar PV system parameter nominal values for one two-module array.

Parameter	Array value (2-modules in parallel)
Maximum power[a], P_{max}, W	380
Maximum power point voltage, V_{mpp}, V	54.8
Maximum power point current[a], I_{mpp}, A	6.94
Open circuit voltage, V_{oc}, V	67.5
Short circuit current[a], I_{sc}, A	7.5
Module efficiency, %	16.1
Solar cell efficiency, %	18.5
Temperature coefficient (P_{max}), %/°C	−0.30
Temperature coefficient (V_{oc} and V_{mpp}), V/°C	−0.169
Temperature coefficient (I_{sc}), mA/°C	0.86
Total module area[b], m^2	2.358

[a] This is two times the nominal values at standard test conditions (irradiance = 1000 W m^{-2} and module temperature = 25 °C) reported by the manufacturer [22].
[b] This is two times the module area reported by the manufacturer [22].

2.1. Solar arrays

The solar arrays have been described previously [12]. In brief, there are four arrays, with each of the arrays containing 10 Sanyo HIP-190BA3 modules. The modules were wired in parallel, so the output current was equal to that for one module, with the current equal to 40 times a single-module value. However, for the tests discussed in this report, only one or two modules from each of the original arrays were used, because the DC–DC converters (described later) could not handle the current from more two modules under sunny conditions. The electrical output from each array was connected to a DC-DC converter, as described later. The electrical parameters for an array are given in Table 1. A picture of the arrays and the charge controller box are shown in Fig. 1. The solar array tilt angle (measured with respect to the ground) was set to the site latitude plus 15° (42° plus 15° = 57°) for this study to optimize the solar energy collection in the winter.

2.2. DC–DC converters

Because the solar arrays had the individual modules wired in parallel, providing a nominal voltage of 50 V at a typical module

Fig. 1. Picture showing the solar PV battery charging system at the GM Milford Proving Ground. The four arrays have a tilt angle equal to the site latitude plus 15° (57° with respect to the earth's surface). The DC–DC converter box is on the cart in the foreground.

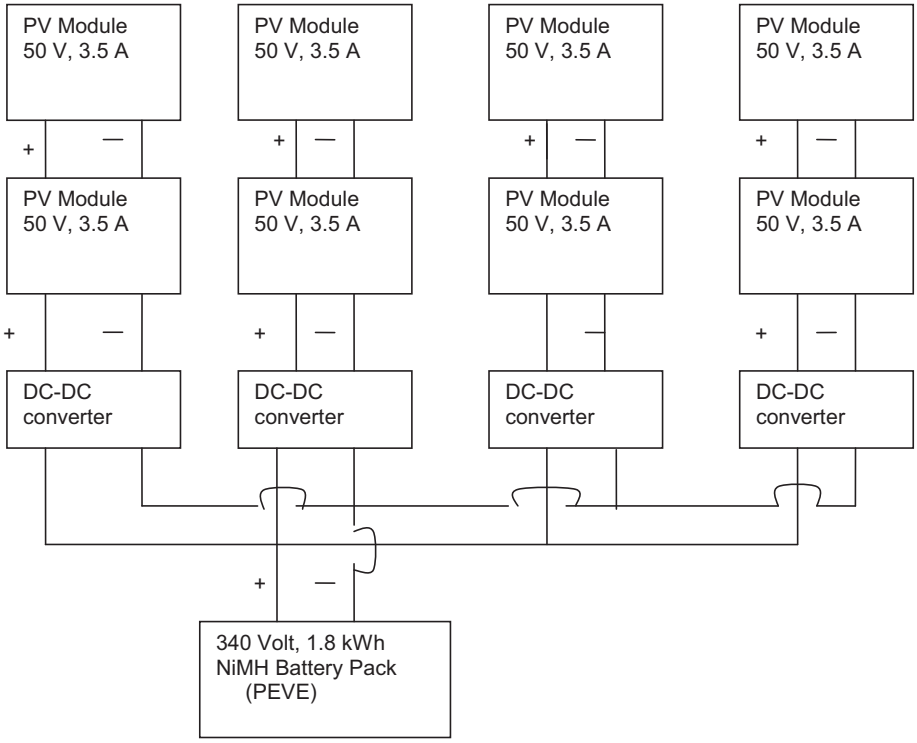

Fig. 2. Schematic of the battery charging system showing four solar arrays, with each array having two modules in parallel. The output of the four DC–DC converters was combined and connected to the NiMH battery terminals.

temperature of about 50 °C, it was necessary to boost the voltage significantly to charge a 300 V hybrid electric vehicle (HEV) battery. This was accomplished using four DC–DC converters (DCC). The DCC were made to our specifications by Solar Converters, Inc. (Guelph, Ontario), Model CV 48/300-1PV 48 R300. A schematic showing the wiring of the PV and DCC systems is shown in Fig. 2. Each DCC accepts the nominal 50-V PV input voltage and output a voltage of up to 350 V for charging the battery. Four identical DCC were used in the study because we were unable to find one single unit that could output sufficient current. Therefore, we took advantage of our multiple-array system (originally designed for an electrolyzer) to make H_2 [12] and utilized one DCC per array. Initially, the DCC output voltages were set to 340 V and the DCC units included charge control at this voltage level. However this limit was increased to 350 V so that the battery charging algorithm (described later) rather than the charge control in the DCC determined when to terminate battery charging. In this way, the DCC acted as boost DC–DC converters, i.e., they boost the nominal 50 V PV voltage up to approximately 350 V to charge the battery.

2.3. NiMH battery pack

A new battery was purchased and used for the tests described in this study. The battery is the Panasonic NiMH battery used in the GM-2-mode hybrid system (Panasonic EV Energy Co. – PEVE) [23,24]. The battery pack, often referred to as the PEVE battery, is similar to the battery pack used in the Toyota Prius, except it has more modules (40 prismatic modules vs. 38 in the Prius) connected in series, and thus slightly higher voltage and energy storage [23]. The 40 prismatic modules in the battery pack had six prismatic NiMH cells per module and two modules per block (total of 20 blocks). Battery parameters were measured and reported by the internal battery pack control module at the block level. For example, the voltage of each block was measured, and the maximum and minimum were used to determine when to stop discharging or charging the battery, respectively. A picture of the two battery packs, hardware associated with controlling the internal battery connectors, a load bank for battery discharging, and a computer for controlling the battery discharging and charging is shown in Fig. 3. The BPCM broadcasts important battery parameters on the CAN bus, and the bus is monitored via an 18-pin connector as discussed later. The BPCM also supports the automatic fan cooling the battery pack and controls the internal battery high-voltage contactors disconnect.

Some relevant nominal values for the battery modules and pack are listed in Table 2. The battery pack [24] consists of: (1) the metal case, (2) the 40 modules, (3) an electronic control module referred to as the battery pack control module (BPCM), (4) interconnecting wires, (5) vents, (6) a cooling fan for air circulation (normally not on – controlled by the BPCM), sensors for measuring important battery parameters, and (7) data communication lines. The BPCM is

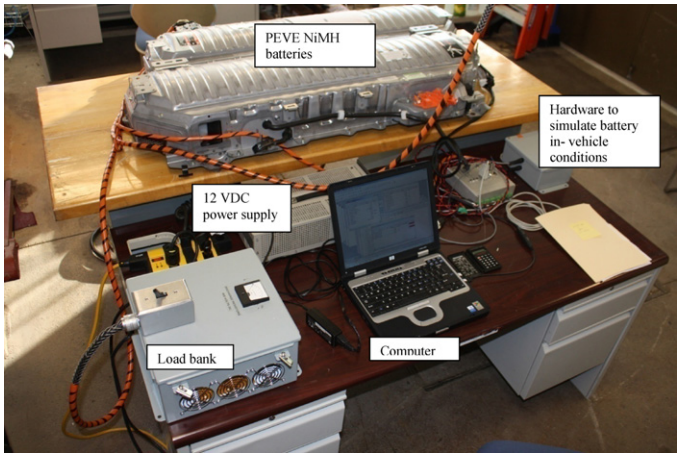

Fig. 3. A picture of two Panasonic (PEVE) NiMH batteries and associated equipment used in the battery discharging and charging experiments.

Table 2
Specifications for GM 2-mode hybrid, energy storage system (NiMH battery pack) [23,24].

Specification	Value
Cell chemistry	NiMH
Module type	Plastic case prismatic
No. cells/module	6
Nominal cell voltage, V	1.2
Nominal module voltage, V	7.2
No. modules/pack	40[a]
No modules per block	2
Module energy density, Wh/kg	46
Module specific power, W kg^{-1}	1300
Module mass, kg	1.04
Module dimensions, cm	1.96 (W) × 10.6 (H) × 28.5 (L)
Pack operational voltage, V	240–340 (see discussion)
Pack voltage limits, V	216–390 (GM specification)
Pack energy capacity, kWh	1.8
Pack charge capacity, Ah	6.5
1 C discharge/charge rate, A	6.5
Pack mass, kg	~67

[a] Sets of two modules were wired into blocks, so there were 20 such blocks in a pack. Block voltages and temperature were individually monitored.

subservient to the vehicle electronic control module (ECM), and we had to provide hardware and software to simulate the conditions the battery would encounter if it were hooked up to the GM 2-mode hybrid ECM. That system will now be described.

2.4. Battery pack activation hardware and software

To charge or discharge the PEVE, the internal high voltage contactors need to be activated so that the terminals are "live". The first step in this process is installing the manual high voltage safety interlock connectors (HVIL); one is present on the battery terminal cover, and a second safety interlock is inserted and locked in on the side of the battery case, below the output terminals. The second step involves waking up the pack and closing the internal contactors by satisfying the battery pack control module (BPCM) criteria that were programmed into the BPCM memory for the pack installed in a GM 2-mode hybrid vehicle. The battery pack has an 18-pin connector, and several of those pins need to have voltages and signals in order for the BPCM to command the pack to wake up and to close the contactors within the battery pack. The hardware to do this consisted of: (1) a 12 V power supply to simulate the low-voltage battery in the GM-2-mode hybrid vehicle, and (2) a pulse generator with the appropriate frequency, pulse width modulation, and duty cycle to simulate the vehicle electronic control module that communicates with the BPCM, and (3) a capacitive load needed at battery-pack contact closure to simulate the battery pack placement with a 2-mode hybrid vehicle. The communication is made through the CAN bus terminals on the connector. The communication is bi-directional; commands are sent to the BPCM and battery data is transmitted from the BPCM. The communication was controlled and parameters from the battery were recorded using a Hewlett Packard model NC600 Laptop computer running CANoe software (Vector CANtech, Novi, MI) described later.

2.5. NiMH battery chemistry

The chemical reactions at the electrodes of a single cell during battery charging are as follows [25–28]:

Positive electrode (anode) :

$$Ni(OH)_2 + OH^- \rightarrow NiOOH + H_2O + e^- \quad (1)$$

Table 3
Important battery pack usage parameters for the NiMH battery pack while under control of the BPCM/CAPL program.

Parameter	Low value (discharge)	High value (charge)
Pack voltage, V	240	340
Block (2-module in series) voltage, V	12	17
Block temperature, °C	2	38

Negative electrode (cathode) reaction :

$$M + H_2O + e^- \rightarrow MH + OH^- \quad (2)$$

where NiOOH is nickel oxyhydroxide, and M the hydrogen absorption alloy (typically a Misch metal).

The standard potentials of the two reactions are E^0 (Eq. (1)) = −0.52 V and E^0 (Eq. (2)) = −0.83 V, so the overall open circuit voltage under standard conditions is 1.35 V. The system is designed so that oxygen gas is released at the anode when the battery is overcharged, and the oxygen diffuses to the cathode where it combines with hydrogen to form water, releasing heat. Provided that the overcharge is mild, this mechanism protects the battery from damage.

The charging voltage is in the range 1.4–1.6 V per cell. A fully charged cell measures 1.4–1.45 V, and supplies a nominal 1.25 V during discharge down to approximately 1 V. Over discharging can lead to polarity reversal of a cell, resulting in hydrogen generation at the positive electrode. As long as the process does not go too far, the hydrogen will diffuse to the negative electrode where it will react with oxygen to form water and release heat. Small amounts of hydrogen and oxygen can be contained within the battery pack case.

2.6. Battery pack control program

The Vector CAN Access Programming Language (CAPL), a programming language used by CANoe, was used to create a customized program to control the PEVE wakeup and contact closure. In battery discharge or charge tests, CANoe first was started, followed by loading the CAPL program. The PEVE wakeup command was then given, and once the pack was awake, the contactors were closed so the battery terminals were "live". In addition, CAPL was used to set important BPCM parameters that assured a safe and useful change in the battery state of charge upon charge or discharge.

The discharge/charge parameters were set in collaboration with GM engineers with experience in charging the PEVE. Table 3 lists the important parameters and the values that were set in the CAPL program. These parameters are based on GM experience with the usage limits of the battery pack and specifications set in consultation with the battery pack manufacturer. When any parameter fell outside the window shown in Table 3, the program opened the contactors and terminated whatever process was occurring (battery discharge or charge). For example, if the battery was being discharged, and the minimum block (2-modules in series) voltage fell below 12 V, the contactors were opened and the discharge was terminated. If all 20 blocks were perfectly balanced, the pack voltage would reach a minimum of 240 V on discharge and 340 V on charge before the CAPL program would open the contactors and terminate the function. Due to the tolerance of NiMH batteries to moderate overcharging [21,29,30], a block-level control (Table 3) is sufficient to safely charge the pack. However, the discharging and charging protocol used in our study, in particular the sustained discharge followed by a sustained charge, is very different than that experienced by the NiMH battery in a hybrid electric vehicle, and

this could adversely affect the battery lifetime. We did not investigate the long-term effect of our discharge/charge protocol on the battery performance.

2.7. Battery discharging and charging protocol

Typically, the battery was discharged using a load bank (described below) until the contactors opened. SOC was not estimated as estimating SOC for NiMH batteries is very difficult [29–32]. Rather we used a simple discharge/charge protocol developed in consultation with GM battery hybrid vehicle engineers. For a discharge experiment the battery high-voltage contactors opened and the test was terminated when one 2-module block voltage fell below the threshold value in Table 3 (12 V) or when the total pack voltage fell below 240 V. Since the pack was new, there was good balance between the 20 2-module blocks, so the pack voltage approached 240 V when the discharging experiment was terminated. Typically, within in an hour of completing a battery discharge test, a battery charging test, using the solar charging system was begun. The charging experiment progressed until one of the 2-module block voltages exceeded the upper threshold in Table 3 (17 V) or when the total battery pack voltage exceeded 340 V, at which point the battery high-voltage contactors opened and the charging experiment was terminated.

2.8. Resistive load bank for battery discharging

A resistive load bank was designed to discharge the battery at an approximately *C*/3 rate. Since the nominal battery voltage was 300 V, and the charge capacity was 6.5 Ah, a resistance of approximately 150 Ω was needed. Three 470 Ω, 300 W Arcol oil-filled resistors (Mouser Electronics) were connected in parallel to make a 157-Ω load bank capable of dissipating 900 W of power. The power resistors were mounted in a box (Fig. 3) with three cooling fans to cool the resistors by circulating room air over them. This system discharged the battery at a current of approximately 2 A.

2.9. Data acquisition

Two data acquisition systems were used to collect the data from the solar and battery systems. One data acquisition system, LABview, was used to collect data from the solar arrays (voltage, current, solar irradiance, solar array temperature). This system is described in detail elsewhere [12].

A second data acquisition system (CANoe) was used to collect data from the PEVE battery (as well as to wake up the battery, close the battery contactors, and control the BPCM, as discussed earlier). This system consisted of hardware (CANcardXL) plugged into the PCMIA port on a Hewlett Packard Laptop computer, a cable (Vector model 251 opto CANcab cable) from the CANcardXL to the 18-pin connector on the PEVE battery, and software (CANoe) to communicate with the BPCM. The variables from the battery were obtained from the BPCM and were obtained from the CAN bus exiting the battery via the 18-pin connector. The variables included pack voltage, pack current, maximum module voltage, minimum module voltage, maximum module temperature, and minimum module temperature. The internal sensors in the battery pack and the CAN bus, along with the data logging features in CANoe were used to record the instantaneous values for these parameters once per second. The LABview system recorded the solar variables once per second, and the two computer clocks were synchronized to the nearest second. This allowed the two data sets to be merged to create the overall databases for analysis of the response of the battery to the solar energy and solar PV electrical power used to charge the battery. The data was exported from CANoe to a comma-delimited data set and read into Excel. The LABview data was also read into Excel and combined with the CANoe data for analysis.

Table 4
PEVE current measurements by the internal sensor in the NiMH battery pack.

Actual current, A	PEVE current	Relative error
0.75–1.249	1.0	−33.3 to +20.0
1.25–1.749	1.5	−20.0 to +14.2
1.75–2.249	2.0	−14.2 to +10.1
2.25–2.749	2.5	−10.1 to +9.1
2.75–3.249	3.0	−9.1 to +7.7
3.25–3.749	3.5	−7.7 to 6.7
3.75–4.249	4.0	−6.7 to + 5.9
4.25–4.749	4.5	−5.9 to + 5.3
4.75–5.249	5.0	−5.3 to +4.8

2.10. Calibration of the voltage and current measurements from LABview and CANoe

The voltage and current measurements from both systems were compared to calibrated Fluke meters maintained in our laboratory. For the CANoe measurements, the Fluke meters were put in-line (current) or across the battery electrodes (voltage) during charging and discharging the battery, and the *V* and *I* values from the meters and from the PEVE were recorded and put into a linear regression. For LABview, the Fluke meters were put in-line or across the solar array input to the DCC during a battery charging experiment. The recorded simultaneous *V* and *I* readings from the Fluke meters and LABview were regressed to obtain the correspondence between the two measures. This comparison accomplished two important objectives: (1) the LABview and CANoe measurements were tied to a single set of standards, and (2) it allowed us to understand the unique characteristics of the PEVE current measurement, that we will discuss in more detail below.

The voltage from each system agreed with the standard meters to better than 1% over the range of voltages measured. The solar array currents also showed such good agreement with the standard meters. The PEVE current was in good agreement over the range of current measurements, but it had a resolution of only 0.5 A (the PEVE BPCM rounded the current to the nearest 0.5 A, and that is what is transmitted down the CAN bus to the CANoe data logging system). The effects of this round off by the BPCM can be understood by referring to Table 4.

At current readings over 1 A, the relative error is less than 20%, and for readings over 3 A, the error is less than 10%. Also, over time the overshoot and undershoot errors should tend to cancel each other. We will return to this topic when we discuss the power and energy balance for the solar and battery energy in the results section.

3. Results and discussion

3.1. Battery pack and solar measurements and calculations

3.1.1. Computations of battery pack changes in electrical energy and charge

The energy added to or removed from the battery pack (ΔE) during the 1-s data collection time intervals (Δt) in our experiments was calculated from the voltage (V), current (I) according to Eq. (1):

$$\Delta E \quad \text{battery pack}, \quad \text{Wh} = V_{batt} \times I_{batt} \times \frac{\Delta t}{3600} \tag{3}$$

The total energy added to the battery over a charging or discharging experiment was calculated by summing the individual

ΔE values over the experimental run. Note that $\Delta t/3600$ has units of h.

The charge added was computed in a like manner from the charge added over a 1-s interval ($\Delta Q = I_{batt} \times \Delta t/3600$), and summing ΔQ over a charging or discharging experiment to get the total charge added in Ah.

The charging and discharging experiments covered an operational range between a fully discharged and a fully charged state for the battery as defined by the voltage limits used in Table 3.

3.1.2. Solar energy and solar electrical measurements during battery charging

The solar energy incident on the solar modules over the 1-s time interval Δt was derived by measuring the solar irradiance ($W\,m^{-2}$) with the four LI-COR radiometers, and computing the energy incident on the modules. The formula was:

$$\Delta E \quad \text{solar energy,} \quad \text{Wh} = \text{Solar irradiance,}$$

$$\text{W m}^{-2} \times 1.179\,\text{m}^2 \times \#\ \text{modules} \times \left(\frac{\Delta t}{3600}\right) \tag{4}$$

The ΔE values in Eq. (4) were summed over time that the battery charging experiment was run to get the total solar energy incident on the solar PV modules used in the test.

The solar electrical energy was computed from the average voltage and current measured at each of the arrays used in the experiment, V_{solar} and I_{solar}, respectively over the 1-s interval Δt.

$$\Delta E \quad \text{solar PV} \quad \text{electrical energy,} \quad \text{Wh} = V_{solar} \times I_{solar} \times \left(\frac{\Delta t}{3600}\right) \tag{5}$$

The total solar PV electrical energy input to the DC–DC converters was the sum of the solar PV electrical energy, ΔE in Eq. (5), over the course of a battery charging experiment.

3.1.3. Solar energy and solar PV electrical energy to battery charge efficiency calculations

Using Eqs. (3)–(5), we can define three efficiencies that define the individual components of the solar to battery charging efficiency. First, the efficiency of the PV solar energy conversion to PV electrical energy is derived from the solar PV electrical energy in Eq. (5) divided by the total solar energy incident on the PV modules in Eq. (4):

$$\text{PV solar energy to PV electrical efficiency,} \quad \% = 100\% \times \frac{\Delta E \quad \text{PV} \quad \text{electrical solar energy,} \quad \text{Wh}}{\Delta E \quad \text{solar energy,} \quad \text{Wh}} \tag{6}$$

Second, the efficiency of the DC–DC conversion process was computed. The electrical energy generated by the solar system is fed to the DC–DC converters where the voltage is boosted to 350 V for battery charging. Some energy is lost in this conversion process. The DC–DC conversion efficiency can be computed as the electrical energy fed to the battery pack, ΔE in Eq. (3), divided by the electrical solar energy generated by the PV system, ΔE in Eq. (5):

$$\text{DC–DC converter efficiency,} \quad \% = 100\% \times \frac{\Delta E \quad \text{battery pack,} \quad \text{Wh}}{\Delta E \quad \text{solar PV electrical energy,} \quad \text{Wh}} \tag{7}$$

Third, the solar system to battery charging efficiency was computed as the electrical energy added to the battery pack, Eq. (3), divided by the solar energy incident on the PV modules, Eq. (4):

$$\text{Solar energy to battery charging efficiency,} \quad \% = 100\% \times \frac{\Delta E \quad \text{battery pack,} \quad \text{Wh}}{\Delta E \quad \text{solar energy,} \quad \text{Wh}} \tag{8a}$$

This can also be expressed as the product of the PV efficiency in Eq. (6) and the DC–DC converter efficiency in Eq. (7):

$$\text{Solar energy to battery charging efficiency,} \quad \% = \frac{\text{DC–DC converter efficiency,} \quad \% \times \text{PV efficiency,} \quad \%}{100} \tag{8b}$$

If the solar PV system was perfectly coupled to the battery during charging, then all of the solar electrical energy in Eq. (5), minus that lost in the DC–DC conversion process, would be delivered to the battery. However, the battery terminal voltage changes during charging so even if the PV system were perfectly coupled at the beginning of a test it would not remain coupled in a steady state. We can calculate the maximum PV efficiency from the information in Table 1 together with the measured module temperature, i.e., utilizing the manufacturer provided temperature coefficient describing the change in efficiency as the module temperature changes.

$$\text{Maximum PV efficiency,} \quad \% = 16.1 + \left(16.1 \times \left(-0.3 \times \left(\frac{(\text{module temperature,} \quad ^\circ\text{C} - 25\,^\circ\text{C})}{100}\right)\right)\right) \tag{9}$$

For example, if the module temperature during a test was 25 °C, then the maximum PV solar to electrical efficiency would be 16.1%. For a module temperature of 50 °C, the maximum PV efficiency would be 14.9%.

The ratio of the PV efficiency measured when the system is connected to the battery load, Eq. (6), divided by the maximum PV efficiency yields the coupling factor:

$$\text{Coupling factor} = \text{PV efficiency ratio} = \frac{\text{Measured PV efficiency,} \quad \%}{\text{Maximum PV efficiency,} \quad \%} \tag{10}$$

Finally, we can calculate the PV maximum power point voltage from the manufacturer supplied value, 54.8 V, and the temperature coefficient for that term using the data in Table 1, −0.169 V/°C.

$$V_{mpp}, \quad \text{V at module temperature} \quad T = 54.8 - ((\text{module temperature} \quad T, \quad ^\circ\text{C} - 25\,^\circ\text{C}) \times 0.169) \tag{11}$$

3.2. Battery pack discharging experiments

Prior to the solar charging experiments, the battery was discharged until the contactors opened due to the constraints regarding the minimum module voltage in Table 3 (battery pack voltage fell below 240 V or one of the minimum two-module block voltages fell below 12 V and the contactors opened). Five battery pack discharging experiments were performed to prepare the battery pack for the PV charging tests. The average discharge rate (C-rate) was 0.3 C (approximately a 2 A current for a 6.5 Ah battery). A substantial portion of the nominal battery energy and charge values listed in Table 2 (energy = 1.8 kWh, charge capacity = 6.5 Ah) was removed with the discharging protocol described in Section 2.7. In some discharge experiments, the battery was not fully charged prior to the discharge. Nonetheless, up to 1.4 kWh of energy and 4.6 Ah of charge were removed in a discharging experiment. After a discharging experiment, when the resistive load was removed, the battery open-circuit voltage recovered to higher values, but this was just a "surface" charge. For example, when a second discharge experiment was run on a previously discharged

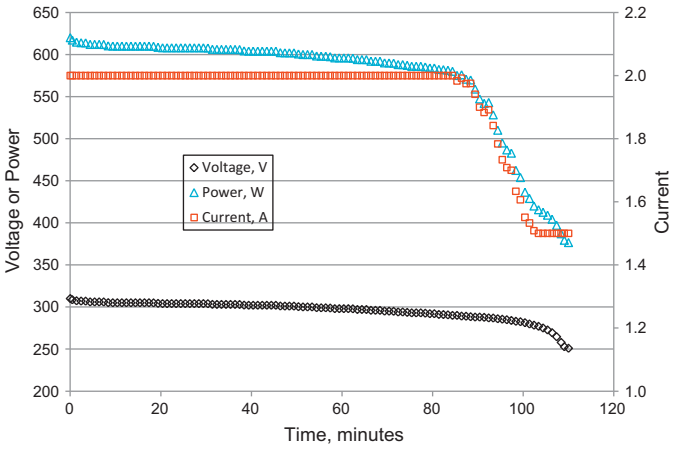

Fig. 4. Results of a battery discharge experiment using the load bank with the discharge limits in Table 4 for an experiment on February 4, 2010. One-min averages, calculated from the 1-s data points, are plotted.

battery, only about 30 Wh of additional energy, and 0.1 Ah of charge were removed after about a 1-h rest period.

A plot of the voltage, current and power versus time for a discharging experiment conducted on February 4, 2010 is shown in Fig. 4. The battery voltage decreased from 310 V to 251 V over the 110-min experiment. The current decreased from 2 A to 1.5 A and the power decreased from 620 W to 376 W. In this experiment 1.05 Wh of energy and 3.52 Ah of charge were removed from the battery pack. The experiment was terminated when one of the battery module voltages fell below 12 V (one of the criteria in Table 3).

3.3. Battery pack charging experiments

3.3.1. Measured DC–DC converter efficiency

The conversion efficiency of the DC–DC converters was determined by using a resistive load bank. The current and voltage through the load bank was measured with Fluke multi-meters, while the solar PV voltage and current were measured with the LABview system. The DC–DC converter efficiency was computed as the ratio of the electrical power out of the DCC and into the load bank, P_{DC-DC}, divided by the solar electric power into the DCC from the PV system, P_{solar}.

We measured a DC–DC converter efficiency of approximately $91 \pm 1\%$ for the four converters using a resistive and to evaluate the system at a power of about 400 W. Direct charging using the solar arrays, wired such that the PV modules would be in series to reach a voltage of 350 V (six to seven modules in series would attain this voltage) would eliminate this loss in voltage conversion, and is planned in a future phase of our testing.

3.3.2. Battery charging tests

A total of six battery charging experiments were conducted over 5 days during the fall of 2009 and the winter of 2010. Table 5 gives a summary of the results. The averages presented in the table utilized 1-s time-resolved measurements of the parameters, and the quantities calculated from the data utilized the 1-s time resolved database. There was a wide variation in the weather conditions experienced during the study. In particular, the solar irradiance ranged from 300 W m^{-2} to 1130 W m^{-2} and the PV module temperature ranged from 15 to 40 °C. The very high solar irradiance on February 8 and February 19 was due to clear, cloud-free conditions enhanced by reflection of direct solar irradiation by snow in front of the solar arrays.

The experiments lasted from 37 to 194 min and utilized either four or eight Sanyo HIP-190BA3 solar modules, together with two or four Solar Converters charge controllers. The charge controllers were adjusted so that they operated as DC–DC converters, i.e., they boosted the low 50 V solar PV voltage to over 340 V DC, but did not control the output voltage or current to the battery. Rather, we used the BPCM and the CAPL program to monitor the battery conditions (see Section 2.6 and Table 3) and to terminate the battery charging by opening the high-voltage contactors within the battery pack case. The BPCM also occasionally turned on an internal fan to cool the battery. However, the BPCM/CAPL program never commanded the battery contactors to open during our charging tests based on battery temperature. Rather all charge terminations commanded by the BPCM/CAPL system were due to the maximum 2-module block voltage exceeding 17 V or the battery pack voltage exceeding 340 V (Table 3). The battery was in a room with an average temperature of approximately 25 °C, and the battery pack maximum module temperature typically remained at room temperature, with only occasional running of the internal battery pack fan.

The average PV voltage into the DC–DC converters (DCC) varied from 45.0 to 58.8 V and the average PV current varied from 5.3 to 22.8 A. These PV voltages and currents in to the DCC resulted in currents into the battery of 1.2–3.8 A (C-rates for from 0.18 to 0.58). The PV MPP voltage, V_{mpp}, was calculated from the values for the Sanyo modules (Table 1) and the module temperature measurements (Table 5). Note, that on February 4, it was colder than the 25 °C temperature at which the STC for the nominal Sanyo specification (Table 1) was obtained. The cold temperature, together with the −0.169 V per °C temperature coefficient (Table 1) increased the calculated V_{mpp} to 56.4 V.

It is interesting that on the day with the lowest solar irradiance, February 4, the DCC operated at a low input voltage, and this was the only day in which the PV output voltage was below the MPP voltage. We also observed this phenomenon, a low PV operating voltage, on other test days during brief cloudy periods. This is believed to be due to the inner workings of the particular DCC design that was used in our tests.

The overall test results over the experiments listed in Table 5 reflect our learning curve in charging the battery. In the first three tests we did not have the charge controllers turned up to a high enough output voltage (348 V) so that the battery BPCM/CAPL system could control termination of the battery charge by opening the contactors when an individual 2-module block voltage exceeded 17 V. For these experiments, charging was terminated when the DCC could not add any more charge to the battery. Also, not shown in Table 5 are several preliminary tests in which the battery parameters such as the maximum and minimum voltages were set so low that only a small amount of energy (approximately 100 Wh) were added before the contactors opened. For the test on February 4, charging was terminated manually because little charge was being added to the battery due to very low solar irradiance as it became very cloudy in the afternoon. For the last two experiments in Table 5 (on February 8 and 19), the charge controllers were adjusted to have a maximum output during sunny periods of 348 V and charging was terminated by the BPCM/CAPL system (the command was prompted by one battery 2-module block exceeding the 17 V threshold). On these 2 days the battery pack maximum voltage reached 340 V.

The total energy added to the battery in Table 5 varied from 0.51 to 1.69 kWh, compared to the 1.8 kWh nominal capacity of the battery in Table 2. The total charge added to the battery pack varied from 1.56 to 5.13 Ah, compared to the nominal charge capacity of the battery in Table 2 of 6.5 Ah. These results show that our discharge/charge protocol resulted in a discharged battery approaching 0% SOC and a charged battery approaching 100% SOC, while still staying within GM-specified limits for the battery parameters in Table 3.

Table 5
Measurements and calculations of the battery charging parameters during six tests conducted over 5 days.

Parameter	Date of experiment					
	Nov. 11, test1	Nov. 11, test2	Nov. 13	Feb. 4	Feb. 8	Feb. 19
Duration of experiment, minutes	47.0	46.9	176.9	195.9	66.3	66.7
Number of solar modules used[a]	8	4	4	8	8	8
Avg. solar irradiance, W m^{-2}	987	890	829	302	1089	1132
Avg. PV module temperature, °C	39.9	40.0	42.1	15.4	43.2	36.9
Avg. PV voltage	58.0	55.2	52.8	45.0	58.8	59.9
Avg. PV current, A	21.9	11.7	10.7	8.9	22.8	22.7
Avg. PV power, W	1269	644	566	400	1342	1362
Total PV electrical energy, kWh	0.99	0.50	1.67	1.31	1.48	1.51
PV V_{mpp}, V	52.3	52.3	51.9	56.4	51.7	52.8
Avg. PV voltage/V_{mpp}	1.11	1.06	1.02	0.80	1.14	1.13
Solar energy input, kWh	7.29	3.28	11.53	9.09	11.35	11.87
Solar PV to electric efficiency, %	13.6	15.3	14.5	14.4	13.1	12.7
Max. solar PV to electrical efficiency, %	15.4	15.4	15.3	16.6	15.2	15.5
Coupling factor	0.89	1.00	0.95	0.89	0.86	0.82
Battery maximum module temperature, °C	23	24	25	24	25	25
Starting battery voltage, V	298	312	284	288	289	295
Ending battery voltage, V	336	333	337	333	340	340
Avg. battery charging current, A	3.6	2.0	1.7	1.2	3.8	3.8
Avg. C-rate, battery charge	0.55	0.31	0.27	0.18	0.58	0.58
Avg. battery charging power, W	1196	653	573	388	1252	1250
Energy added to battery, kWh	0.94	0.51	1.69	1.27	1.38	1.39
Charge added to battery, Ah	2.82	1.56	5.13	3.90	4.19	4.20
DC–DC converter efficiency, %	94	~100	~100	97	93	92
Solar to battery charge efficiency, %	12.8	15.6	14.7	13.9	12.2	11.7

[a] This is total number of PV modules used. Typically two Sanyo PV modules, wired in parallel, from each array were connected to each of four DC–DC converters, for a total of eight PV modules used.

The most important variables with respect to solar charging of the battery are the PV efficiency (solar energy to PV electrical energy efficiency), the DC–DC converter efficiency, and the product of those two quantities, the solar to battery charge efficiency. The solar to electric efficiency varied from 12.7% to 15.3% with a mean value of 13.9%. It was controlled by how well the solar and battery systems were coupled and how close the solar voltage approached the MPP voltage for the PV system, as discussed later. The DC–DC converter (DCC) efficiency over the six experiments varied from 92% to 100% with a mean of 96%. The higher values were measured at the lower battery current measurements where the error in the battery current measurement is highest (see Table 4). At the higher battery currents measured on February 8 and 19 the DCC efficiency was 92–93%. This is in approximate agreement with the DCC conversion efficiency of approximately 91%. This loss in the DC–DC conversion could be avoided by using a series wiring configuration of the PV modules to reach 350 V, and eliminating the DC–DC conversion in future embodiments of our charging system. The overall solar to battery charging efficiency varied from 11.7% to 15.6% with a mean of 13.5%. This is comparable to the 14.5% value obtained in an earlier study directly charging small packs of Li-ion batteries with our solar system [11].

The coupling factor between the PV and battery systems in Table 5 varied from 0.82 to 1.00 with a mean value of 0.90. This shows that the PV system remained near the maximum power point over the battery charging experiment. Interestingly, the mean coupling factor value of 0.90 is similar to the values measured for coupling between our PV system and an electrolyzer to produce hydrogen [9,10,12].

Our two best experiments were those on February 8 and 19. This conclusion is based on the criteria that these experiments had: (1) the highest battery charging current and thus the lowest measurement error in the current variable, and (2) a DCC output voltage setting of over 340 V so the BPCM/CAPL program terminated the charging, i.e., there was no DCC charge control. The results from these two experiments were very similar. For these experiments, the battery was charged with about 1.4 kWh of energy and 4.2 Ah of charge, from starting voltages of about 290 V to a final voltage of 340 V using solar energy. The charging took a little over an hour; the C-rate was about 0.58 and the battery added charge was about 65% of the battery charge capacity. This shows that the discharge/charge protocol we used, with simple voltage limits at the block (2-module) level, yielded significant changes in the state of charge of the battery pack. Regarding the efficiency of the charging process, the PV solar to electrical efficiency was about 13%, and the DC–DC conversion efficiency was over 90%. The overall solar to battery charging efficiency was about 12%.

3.3.3. *Example of a battery charging experiment*

The PV and battery charge voltage and current results for the experiment on February 8 are shown in Fig. 5. Fig. 5a shows a plot of the battery voltage and current, while Fig. 5b shows the solar PV voltage, the PV MPP voltage (calculated from the Sanyo specifications in Table 1), and the total solar PV current into the DC–DC converters as a function of the running time of the experiment. The battery voltage increased from about 289 V to about 340 V over the course of the experiment and the battery charge current decreased form an initial value of approximately 4.5 A to a value of approximately 3.5 A. The solar PV voltage slowly increased during the experiment from approximately 56 V to approximately 60 V, and its deviation from the MPP voltage also increased. The total solar PV current monotonically decreased from approximately 27 A to 22 A.

Fig. 6a shows the solar to battery charging efficiency as well as the two sub-efficiencies, the DC–DC converter efficiency and the PV efficiency, that determine the overall system efficiency for the February 8, 2010 experiment. The overall solar to battery charging system efficiency varied from a high of over 14% at the beginning of the experiment to a low of about 11% at the end. The irregular DC–DC (DCC) converter efficiency variation in Fig. 6a, i.e., the sawtooth pattern, is due to the overshoot–undershoot phenomenon caused by the PEVE current measurements (see Fig. 5a) discussed

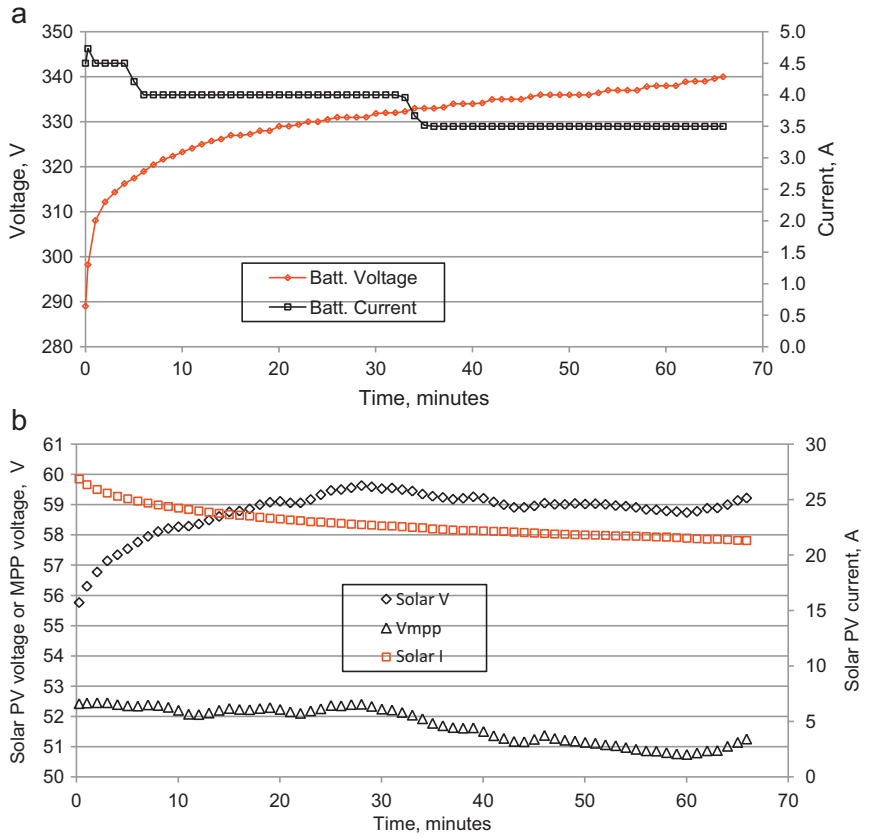

Fig. 5. Results of a battery charging experiment on February 8, 2010: (a) plot of battery voltage and current and, (b) plot of PV voltage, PV MPP voltage (V_{mpp}), and the total PV current into the DC–DC converters. This test was run on a very sunny day.

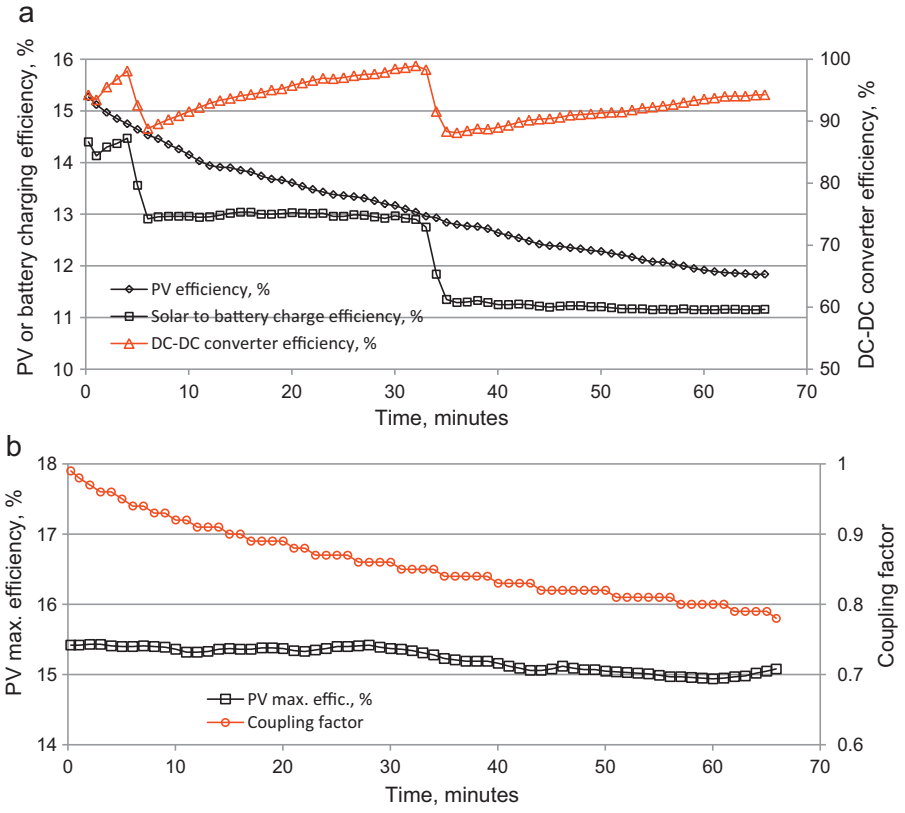

Fig. 6. Results for battery charging experiment on February 8, 2010: (a) measured PV solar to electric efficiency, DC–DC converter efficiency, and overall PV solar to battery charge efficiency, and (b) calculated PV maximum efficiency and PV-battery coupling factor during the charging test.

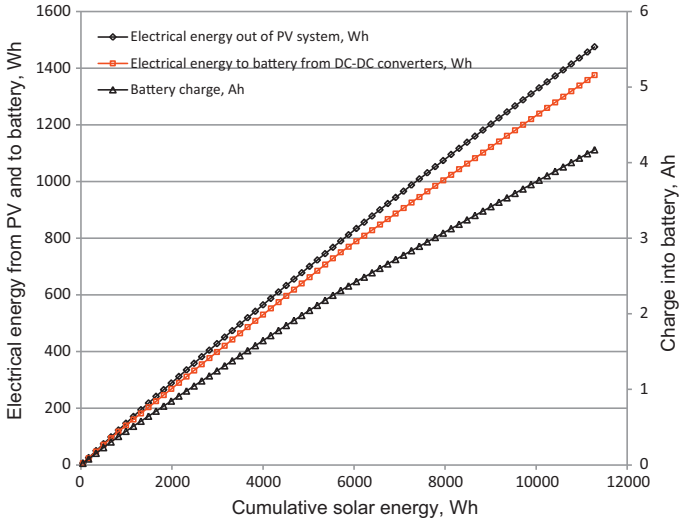

Fig. 7. Cumulative solar electrical energy generated by the PV system, delivered to the battery, and total charge input to the battery as a function of the cumulative solar energy incident on the PV modules used during the test on February 8, 2010.

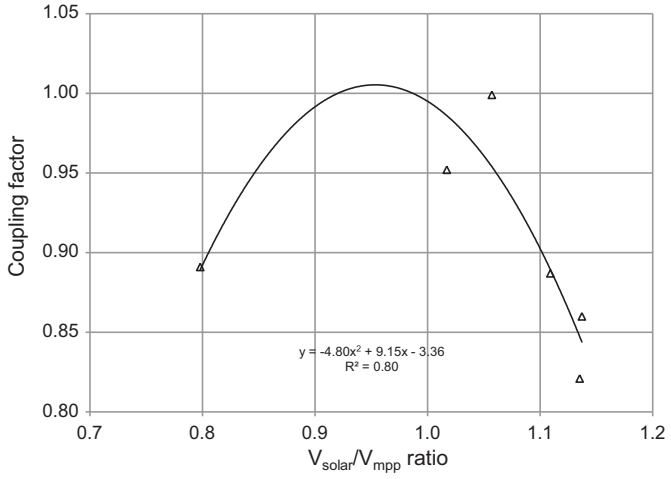

Fig. 8. Dependence of the coupling factor between the PV and battery systems on the V_{solar}/V_{mpp} ratio for the data in Table 5. A polynomial fit trend line is also shown.

earlier (see Section 2.10 and Table 4). The 0.5 A shift in the measured current (Fig. 5a) caused a change in the measured energy going into the battery pack and resulted in the variation in the DCC converter efficiency, computed using Eq. (7), observed in Fig. 6a. This artifact also resulted in the saw-tooth pattern in the overall solar to battery charging efficiency in Fig. 6a. However, this calculated variation in the DCC only has a small effect on the overall battery charging efficiency. The fall-off over time in battery charging efficiency is mainly controlled by the monotonic decrease in the PV efficiency over the experiment. The PV efficiency varied from a high of over 15% at the beginning of the experiment to a low of about 12% at the end. As the battery became charged and the voltage increased (Fig. 5a) a higher PV voltage was needed (Fig. 5b) to drive the charging process. This resulted in a larger difference between the solar PV voltage and the solar PV MPP voltage as time progressed (Fig. 5b), reducing the PV solar to electrical efficiency and the overall solar to battery charging system efficiency observed in Fig. 6a.

Fig. 6b shows the variation in the maximum PV efficiency (Eq. (9)) and the coupling factor (Eq. (10)) between the PV and battery systems. There was a small fall-off in the calculated maximum PV efficiency caused by an approximately 10 °C increase in the temperature of the PV modules over the course of the experiment. This temperature increase resulted in a 1.7 V decrease in V_{mpp} (Fig. 5b) and caused the calculated maximum PV efficiency, using the information in Table 1, to decrease from 15.4% to 14.9% (Fig. 6b). The coupling decreased from a high value near unity at the start of the test to a value of about 0.8 at the end of the test. This decrease in the coupling factor was caused by the increasing gap between the PV operating voltage and the PV MPP voltage (see Fig. 5b), and led to the continuous decrease in the PV solar to electrical efficiency throughout the experiment (see Fig. 6a).

Fig. 7 shows the cumulative solar electrical energy generated by the PV system, the total cumulative electrical energy delivered to the battery, and the total charge delivered to the battery as a function of the cumulative solar energy incident on the PV modules used for the test on February 8. There is a small fall-off in each quantity at higher values of the cumulative solar energy. This effect is minor, and is partially caused by heating of the PV modules that slowly increased their temperature and reduced their voltage output and their solar to electric efficiency (Table 1).

3.3.4. System coupling factor

In earlier work on solar hydrogen and solar battery charging we demonstrated how the coupling between a PV system and a load is very important in determining the system efficiency [9]. This result is due to the unique feature of a PV power system in that its output has a maximum power point and the load characteristics will determine how close the PV system operates relative to that maximum power point. If the load voltage remains near the PV MPP voltage the amount of power transferred to the load (in our case, the battery) will be maximized. Using the data in Table 5 we can determine how well this was achieved during the battery charging experiments. Fig. 8 shows a plot of the system coupling factor versus the important ratio V_{solar}/V_{mpp}. Although there is considerable scatter in the data, the fall-off in the coupling factor to the left and to the right of a V_{solar}/V_{mpp} ratio near unity is clear. Further discussion of the importance of the system coupling factor for hydrogen production and battery charging are given elsewhere [9].

3.3.5. Comparison of energy and charge removed via discharging and added via charging

Due to hysteresis in the charging and discharging, the energy and charge removed in a discharge is not expected to be equal to the energy added on charging for the low (240 V) and high (340) limits put on the battery pack. For three tests in which a battery was fully charged and then fully discharged, the ratio of the charge added to that removed was 1.12 ± 0.06. Batteries with long cycle life like the NiMH battery typically have coulombic efficiencies [33] near unity [26], so the difference reflects hysteresis in the voltage plateaus in the battery charging and discharging protocol [29–32].

3.3.6. Recovery in the battery pack voltage when the load bank of PV charging was removed

In preparation for charging, the battery was typically discharged to a pack voltage of approximately 250 V as shown in Fig. 4 (this voltage corresponded at one block voltage reaching a 12 V minimum). However, in the interim time between the discharge and the solar charging, the battery voltage was observed to recover by 30–40 V. For example, in Fig. 5a, the starting battery voltage was 289 V, although the ending voltage on discharge was 252 V. One question is, how much energy can be removed in a battery that shows this voltage recovery? We determined this in several tests in which a second discharge of a discharged battery was performed. The voltage quickly decreased over a period of about 5 min and the battery internal contactors reopened. Only 30–60 Wh of energy was

removed in such tests. Thus, the voltage recovery is just a surface charge with very little useful energy.

Similarly, after a battery was charged, we attempted a second charge. The contactors opened after a few minutes with the addition of approximately 30 Wh of energy. In conclusion we cannot get much energy or charge into or out of the PEVE battery pack (within the discharge/charge limits we set in Table 3) by doing a second discharge or charge, and the charge limits in Table 3 reflect a practical working voltage range for charging and discharging this battery pack.

3.3.7. Battery heating

The amount of electrical energy converted to heat energy during battery charging can be estimated [34–38] using the data for the first battery charging test on November 11 (Table 5). For this test, the battery fan did not come on to cool the battery during the test, so any heat generated would be realized as a temperature increase in the battery pack. The minimum and maximum block (2-module block) temperatures change during the test differed by 4 °C, and as an upper limit we will assume that the whole battery pack temperature changed by this amount. The heat capacity at constant pressure, C_p, reported for the Prius battery is 976 J kg^{-1} °C or 0.271 Wh/kg °C [36], and the C_p for our battery pack should be similar. For a battery mass of about 67 kg (Table 2), the heat energy generated within the battery is calculated to be approximately 73 Wh versus the 940 Wh of electrical energy added to the battery. Thus, we estimate that less than 8% of the electrical energy was converted into heat in this test. This suggests that little energy is lost as heat in the battery charging process and over 90% of the electrical energy is stored in the battery as charge.

The heat generated by passing current through the internal resistance of the battery can be calculated based on the reported value of 11.4 mΩ/module [27]. For a 40-module pack and a 1 C charging or discharging rate, the I^2R losses are less than 1% of the delivered electrical power. This suggests that very little of the battery heating is due to I^2R losses, and most of the heating, estimated above as less than 8% of the electrical energy added to the battery pack, is due to the overvoltage needed to dive the electrochemical reactions (Eqs. (1) and (2)) to charge the battery.

3.3.8. Parasitic losses

To directly charge the battery with DC, we need to "wake up" the battery pack so that the BPCM is active and measuring and controlling key battery parameters such as module temperature and voltage. This required approximately 12 V and 1 A from a DC power supply. So, when solar power is being added at a rate of $C/2$, power is being added at approximately 900 W, and approximately 12 W of power is being consumed just to keep the BPCM "awake" and the internal battery contactors closed. This is only 1.3% of the solar power, so it is not significant.

When any block (2-module block) temperature exceeded a setpoint, a fan inside the battery was run. This took approximately 5 A of 12 V battery power. So, if the fan was running during the battery charging period, and if the battery was being charged with solar energy at a rate of $C/2$, then the parasitic loss would be 12 V × 6 A = 72 W (BPCM and fan). This is about 8% of the solar power for a worst-case scenario of having the fan running all the time. Even for this case, that is not normally expected, the solar to battery charge efficiency would be lowered from 13.5% (average of six values in Table 5) to 12.4%. Even this worst-case parasitic loss is not significant, and shows that direct solar charging of the high-voltage battery is efficient.

Even a small solar panel on the roof on the vehicle, with only a 200 W output, could be used to charge the high-voltage battery in an EREV or a pure BEV, based on the energy usage of the BPCM and occasional running of the battery fan, provided it had a high voltage output or a DC–DC converter to increase the output voltage. However for such a small system there could be times when the efficiency is significantly reduced due to parasitic losses.

3.4. Comparison of the energy efficiency of solar battery charging to solar hydrogen utilization

The average solar to battery charge efficiency from the data in Table 5 was 13.5%. In a previous study on the generation of high-pressure hydrogen via water electrolysis the efficiency was about 10% based on the LHV of hydrogen (the LHV very close to the standard chemical value of hydrogen – the Gibbs free energy – in an ideal fuel cell). Thus, the solar to battery charge process is about 30–40% more efficient that the solar hydrogen process producing hydrogen. This is mainly due to the overvoltage at the anode for the oxygen evolution reaction in the water electrolysis process. The battery charging process also gains on the hydrogen process in the reverse of the generation process, i.e., battery discharging or usage of hydrogen in a FCEV. While the battery discharge process for NiMH (or especially Li-ion) batteries is nearly 100% efficient in making electrical energy, the hydrogen utilization process in a fuel cell is only about 50% efficient due to losses at cathode for the oxygen reduction process in the fuel cell. Thus, overall, the solar battery charging/discharging process is about 2–3 times as efficient as the solar hydrogen/fuel cell process on an energy basis.

3.5. Possibility of using PEVE batteries in EREV

The PEVE battery pack has only about 1.4 kWh of available energy stored (Table 5); this is about 15% of that available in the Chevrolet Volt battery pack with Li-ion batteries (about 10 kWh of usable energy for a 40 mile range). Thus, it would take about six PEVE battery packs to develop a useful driving range on electric power using PEVE batteries. At present, the trend in vehicles with electric or partially electric powertrains is to use Li-ion batteries. Nonetheless, the NiMH technology remains a viable technology for HEV, EREV, and BEV.

4. Summary

We designed and tested a PV solar battery charging system consisting of low voltage solar modules along with a DC–DC converter to boost the voltage sufficient to charge the 2-mode hybrid GM battery at a rate of $C/2$ (charge the battery with a current equal to 1/2 of its Ah capacity). The battery charging and discharge limits were controlled by the internal BPCM. This design resulted in a simple system with a high solar to battery charging efficiency by keeping the coupling of the solar energy and battery charging near unity. The high efficiency of the battery charging makes this a very attractive use of renewable solar energy as compared to using solar energy to generate hydrogen. On an energy efficiency basis alone, solar battery charging is two to three times as efficient as solar hydrogen generation and usage in a FCEV. The test results prove the concept of PV solar DC charging for plug-in vehicles (extended range electric vehicles) and show that an optimized system regulated by the internal BPCM and some software could be developed for home or commercial recharging systems.

5. Conclusions

1. The high-voltage NiMH batteries used in the large GM 2-mode hybrid vehicles were efficiently charged by direct current from photovoltaic (PV) modules and DC–DC converters to boost the low PV voltage to the high battery charging voltage.

2. The solar energy to battery charging system efficiency averaged 13.5% over six experiments, determined as the product of two sub-efficiencies: (1) a PV system solar to electrical efficiency of 13.9%, and (2) a DC–DC converter efficiency of 90–96%. The coupling factor between the PV and battery systems averaged 0.90, indicating that the PV system power output remained within 10% of the maximum power point.
3. The test results prove the concept of PV solar charging for plug-in vehicles (extended range electric vehicles) and show that a DC system could be used for home or commercial recharging systems with some additional hardware and reprogramming of the battery pack control module.
4. The BPCM can be used to regulate the point at which charging is terminated, effectively making it the charge controller. This makes the design of the DC–DC converter simple as it does not have to control the battery cut-off charging voltage.

Acknowledgments

We wish to acknowledge the following for their valuable help: Carlos Franca, Vance McCabe, Douglas Drauch, Dennis Fowler, Damond Hinatsu, Ryan Kuhlenbeck, Morgan Li, Andres Mituta, Vernon Newhouse, Vance McCabe, David Ouwerkerk, Michael Rogers, Gregory E. Smith, and Ciro Spigno. Special thanks to Vernon Newhouse, Ciro Spigno, Morgan Li, Douglas Drauch, and Michael Rogers for help with the CAPL program, the battery charging algorithm, the Vector software, the battery interface hardware, and LABview programming, respectively.

References

[1] A. Taub, in: Conference on Electrifying Transportation, presented at the North Carolina Solar Center, North Carolina State University, May 27, 2009.
[2] L.D. Burns, in: The 5th IEEE Vehicle and Power Propulsion Conference (VPPC09), September 7–11, 2009, Dearborn, MI.
[3] L.D. Burns, J.B. McCormick, C.E. Borroni-Bird, Scientific American 287 (2002) 64–73.
[4] S. Campanari, G. Manzolini, F.G. de la Iglesia, Journal of Power Sources 186 (2009) 464–477.
[5] P. Gifford, J. Adams, D. Corrigan, S. Venkatesan, Journal of Power Sources 80 (1999) 157–163.
[6] K.A. Snyder, X.G. Yang, T.J. Miller, Hybrid vehicle battery technology – the transition from NiMH to LI-ion, SAE Paper 2009-01-1385.
[7] G. Fontaras, P. Pistikopoulos, Z. Samaras, Atmospheric Environment 42 (2008) 4023–4035.
[8] DOE, Energy Storage Research and Development, January, 2009, www1.eere.energy.gov/vehiclesandfuels/pdfs/program/2008_energy_storage.pdf.
[9] N.A. Kelly, T.L. Gibson, M. Cai, J.A. Spearot, D.B. Ouwerkerk, International Journal of Hydrogen Energy 35 (2010) 892–899.
[10] T.L. Gibson, N.A. Kelly, International Journal of Hydrogen Energy 33 (2008) 5931–5940.
[11] T.L. Gibson, N.A. Kelly, Journal of Power Sources 195 (2010) 3928–3932.
[12] N.A. Kelly, T. Gibson, D.B. Ouwerkerk, International Journal of Hydrogen Energy 33 (2008) 2747–2764.
[13] G.W. Crabtree, N.S. Lewis, Physics Today 60 (2007) 37–42.
[14] J.A. Turner, Science 305 (2004) 972–974.
[15] J.A. Turner, G. Sverdrup, M.K. Mann, P.C. Maness, B. Kropski, M. Ghirardi, R.J. Evans, D. Blake, International Journal of Energy Research 32 (2008) 379–407.
[16] National Research Council/National Academy of Engineering, Hydrogen Economy: Opportunity, Costs, Barriers, and R&D Needs, National Academy Press, Washington, DC, 2004.
[17] D. Ipsakis, S. Voutetakis, P. Serferlis, F. Stergiopoulos, C. Elmasides, International Journal of Hydrogen Energy 34 (2009) 7081–7095.
[18] D.P. Birnie III, Journal of Power Sources 186 (2009) 539–542.
[19] H. Hoshino, H. Uchida, H. Kimura, K. Takamoto, K. Hiraoka, Y. Mausumae, International Journal of Hydrogen Energy 26 (2001) 873–877.
[20] W. Kempton, J. Tomic, Journal of Power Sources 144 (2005) 280–294.
[21] G. Gutmann, Journal of Power Sources 84 (1999) 275–279.
[22] Sanyo Energy (USA) Corp., HIT Series Data Sheet, HIP-190BA3, us.sanyo.com/solar/.
[23] PEVE, www.peve.jp/e/hevknnoku.html.
[24] Damond Hinatsu, General Motors Systems Engineering, Personal Communication.
[25] D. Linden, D. Magnusen, in: D. Linden, T.R. Reddy (Eds.), Handbook of Batteries, Third Edition, McGraw Hill, 2002 (Chapter 29).
[26] M. Fetcenko, in: D. Linden, T.R. Reddy (eds.), Handbook of Batteries, Third Edition, McGraw Hill, 2002 (Chapter 30).
[27] J. Yamaguchi, Toyota Prius: AEI best engineered vehicle 2004, AEI Engineering News, March 2004, pp. 58–68.
[28] A. Taniguchi, N. Fujioka, M. Ikoma, A. Ohta, Journal of Power Sources 100 (2001) 117–124.
[29] M. Verbrugge, P. Liu, Journal of Power Sources 174 (2007) 2–8.
[30] M. Thele, O. Bohlen, D. Uwe Sauer, E. Karden, Journal of Power Sources 175 (2008) 635–643.
[31] M. Verbrugge, J. Tate, Journal of Power Sources 126 (2004) 236–249.
[32] X. Tang, X. Zhang, B. Koch, D. Frish Model-based estimation of nickel metal hydride battery hysteresis for SOC estimation, Proceedings of International Conference on Prognostics and Health Management Denver CO 2008.
[33] A.J. Smith, J.C. Burns, S. Trussler, J.R. Dahn, Journal of the Electrochemical Society 157 (2010) A196–A202.
[34] A. Pesaran, Journal of Power Sources 110 (2002) 377–382.
[35] A. Pesaran, A. Vlahinos, T. Stuart, in: 6th ASME-JSME Thermal Engineering joint Conference, March 16–20, 2003, TED-AJO3-633.
[36] T. Stuart, F. Fang, X. Wang, C. Ashtiani, A. Pesaran, A modular battery management system for HEVs, SAE Paper 2002-10-1918.
[37] A. Pesaran, M. Keyser, in: Annual Battery Conference: Advances and Applications, Long Beach, CA, January 9–12, 2001 (he says C_p = 521 J/kg C).
[38] K.J. Kelly, M. Mihalic, M. Zolot, Battery usage and thermal performance of the Toyota Prius and Honda Insight for various chassis dynamometer test procedures, NREL report NREL/CP-540-31306, November 2001.